PCCP

PAPER

View Article Online
View Journal | View Issue

Cite this: *Phys. Chem. Chem. Phys.*, 2019, **21**, 11011

Received 21st September 2018,
Accepted 26th April 2019

DOI: 10.1039/c8cp05946b

rsc.li/pccp

The role of pH, metal ions and their hydroxides in charge reversal of protein-coated nanoparticles†

Jonas Schubert, *[ab] Carmen Radeke,[a] Andreas Fery[ab] and Munish Chanana *[cd]

In this study, we investigated charge inversion of protein-coated Au nanoparticles caused by the addition of metal ions. The addition of hydrolyzable metal ions (Lewis acids) can induce drastic pH changes and depending on this pH, the metal ions (*e.g.* M^{3+}) are readily converted into the hydrolyzed species (MOH^{2+}, $M(OH)_2^{+}$) or even into hydroxides ($M(OH)_3$). Adsorbed metal hydroxides were identified to cause the charge inversion of the NPs by using a combination of cryo-TEM, EFTEM and ζ-potential measurements.

1. Introduction

The phenomenon of charge inversion (*i.e.* overcharging, charge reversal) has always been controversial and is still under discussion as "unambiguous experimental evidence is virtually non-existent".[1] Up to now, there are several theories at hand.[2]

Whereas the physical approaches explain the charge inversion *e.g.* by ion–ion correlation mechanisms,[1,3] the chemical theories assume that a super-equimolar adsorption of oppositely charged species is the cause.[1,2,4]

In the case of negatively charged proteins, oppositely charged species can either be protons (pH), metal cations or metal hydroxides.[1,2,5] Charge inversion by pH is manifested in the isoelectrical point of proteins. What remains unclear is the origin of charge inversion when metal ions are added: it is either caused by metal ions or by metal hydroxides.[1,2] It is however a well-known fact that charge inversion can only be observed for hydrolyzable metal ions (mostly transition metal ions).[6] This means that at a specific pH the metal ion (*e.g.* M^{3+}) converts into its hydrolyzed species (MOH^{2+}, $M(OH)_2^{+}$) or even its hydroxides ($M(OH)_3$).[7] As the surface charge of these hydroxides depends on the pH as well, the pH seems to be the one key parameter that enframes all interactions.[8]

In literature, charge inversion is either attributed to the adsorption of unhydrolyzed ions,[9–24] hydrolyzed ions[25–33] or hydroxides.[34–36] Which of these species is eventually responsible, remains unclear because the commonly used electrophoretic measurements (*e.g.* ζ-potential measurements) alone cannot distinguish between these three species.[1,2,6]

Therefore, the identification and localization of the adsorbing species (the adsorbate) is crucial. To localize the adsorbate, the adsorbent (*i.e.* proteins) needs to be localized, as well. As the localization of proteins with TEM is a challenging task, immobilized bovine serum albumin (BSA) on Au NPs was applied as adsorbent in this study. Due to the high contrast of Au NPs in TEM, both, the fixed adsorbent (protein) and the adsorbate are therefore identifiable and localizable with TEM. Furthermore, the plasmonic properties of Au NPs allow it to study the influence of the metal species on the colloidal stability as the color of Au NPs changes when aggregation occurs.

2. Results

Au@BSA NPs were synthesized by coating citrate-stabilized Au NPs (Au@citrate) with BSA through ligand exchange, according to the method we previously reported on ref. 24 and 37–43. The average size of the Au@citrate NPs was 15 ± 2 nm. The as-prepared Au@citrate NPs were added to a BSA solution (0.1% citrate, pH ≈ 9) at room temperature and stirred for 24 hours. The NPs were purified from protein excess and concentrated (5–10 mM Au) by fivefold centrifugation (*cf.* more details in the Experimental section). The resulting Au@BSA NPs exhibited an LSPR band, at around 525 nm, *i.e.* a red shift of 2–3 nm compared to the original citrate-stabilized Au NPs, due to the refractive index changes in the vicinity of Au NPs.

Due to the protein coating, the Au@BSA NPs exhibit a pH-responsive reversible aggregation/disaggregation behavior. At pH values close to the pI of BSA (4.7 [44,45]), Au@BSA NPs consistently aggregate and change their color from red over violet/purple to grey/blue. The plasmon band of the NPs' dispersion

[a] *Leibniz Institute of Polymer Research Dresden, 01069 Dresden, Germany. E-mail: schubert-jonas@ipfdd.de*
[b] *Physical Chemistry of Polymer Materials, Technische Universität Dresden, D-01062 Dresden, Germany*
[c] *Institute of Building Materials, ETH Zürich, 8093, Zürich, Switzerland. E-mail: chananam@ethz.ch*
[d] *Department of Physical Chemistry II, University of Bayreuth, 95447 Bayreuth, Germany*

† Electronic supplementary information (ESI) available. See DOI: 10.1039/c8cp05946b

becomes broader and shifts to longer wavelengths.[37,40] Aggregation can also be induced by the addition of metal ions because repulsive charges are screened.[24,46] In previous results, we investigated the interaction of Au@insulin and metal ions. Therein, we stated that overcharging was caused by the adsorption of ions.[24]

In this publication, we took a more precise look at the pH change by adding metal ions and at the influence of the metal hydroxide formation on the charge of the Au@BSA NPs. For this purpose, the interactions of Au@BSA NPs with different di- and trivalent metal ions were investigated. We selected the two alkaline earth metal ions Mg^{2+} and Ca^{2+} as divalent ions as well as the most commonly investigated transition metal ions, *i.e.* Mn^{2+}, Fe^{2+}, Co^{2+}, Ni^{2+}, Zn^{2+} and Cu^{2+}, and the toxic heavy metal ions Pb^{2+}, Cd^{2+} and Hg^{2+}. For the case of trivalent ions, we selected Al^{3+} as a main group metal ion and Fe^{3+}, Cr^{3+}, Au^{3+} and La^{3+} as transition metal ions.

To allow a comparison between this and the previous publication's data, the pH was adjusted to 7.4. Then the ions were added to a final concentration of 100 μM and the pictures were taken after 30 min of incubation. Then the pH and the ζ-potential were measured.

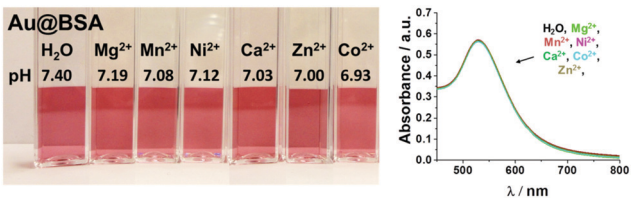

Fig. 1 Optical response of Au@BSA NPs towards divalent metal cations. Photographs and respective UV-Vis spectra of dispersions of Au@BSA in the presence of various divalent cations confirmed the maintained stability indicated by the sustained red color. The cuvettes were sorted by decreasing pH from 7.4 to 6.9. The NP concentration for all dispersions was 0.15 mM Au(0) and the cation concentration was 100 μM. The photographs and the UV-Vis spectra were taken 30 min after the addition of the cations.

The cuvettes were organized with respect to their response and the resulting pH. In Fig. 1, Au@BSA dispersions are shown, which remained stable after the addition of the divalent metal ions (Ca^{2+}, Mg^{2+}, Co^{2+}, Ni^{2+}, Mn^{2+}, Zn^{2+}), *i.e.* they kept their original red color and the LSPR band was unchanged. The pH changed only very little from 7.4 down to 6.93.

In contrast to this, Fig. 2 shows the Au@BSA NP dispersions, that interact with some of the divalent ions (Cd^{2+}, Hg^{2+}, Cu^{2+}, Pb^{2+}, Fe^{2+}) as well as with the trivalent ions (La^{3+}, Cr^{3+}, Al^{3+}, Au^{3+}, Fe^{3+}). The optical response towards Fe^{2+} and Cd^{2+}, Fe^{3+}, Al^{3+} and Cr^{3+} was very weak and the LSPR band red-shifted only very slightly, whereas the particle systems showed a spontaneous color change from purple/blue to bluish grey in the presence of Hg^{2+}, Cu^{2+}, Pb^{2+}, La^{3+} and Au^{3+} (Fig. 2), thus indicating strong aggregation of the NPs.

The pH changed from 7.4 to 7.00–5.25. The addition of Au^{3+} changed the pH to the isoelectrical point – for Fe^{3+}, the isoelectrical point was even exceeded. The strong change in pH stems from the ion specific Lewis acidity.

In order to detect overcharging and to get insight into the electrostatic stabilization of colloids, we conducted ζ-potential measurements (Fig. 3). As stability threshold we applied ±25 mV, which is common practice because it represents a Coulomb energy of $1kT$, *i.e.* the average kinetic energy of a charged particle. Therefore it solely applies for electrostatically stabilized NPs.[47] As steric repulsion contributes to the stabilization of Au@BSA NPs as well, it serves as an orientation here (*cf.* Fig. 3 red dotted lines).[48,49]

From Fig. 3A we can see that the ζ-potential for Au@BSA NPs at pH 7.4 and at low ionic strength is beyond −40 mV, indicating high surface charge and therefore high colloidal stability. In the presence of Mg^{2+}, Mn^{2+}, Ni^{2+}, Ca^{2+}, Zn^{2+}, Co^{2+} and Cd^{2+}, the ζ-potential of the NPs decreases to the stability threshold of −25 mV. This confirms the colloidal stability of the Au@BSA NPs, which is indicated by the red color of the dispersions (*cf.* Fig. 1). For Cu^{2+},

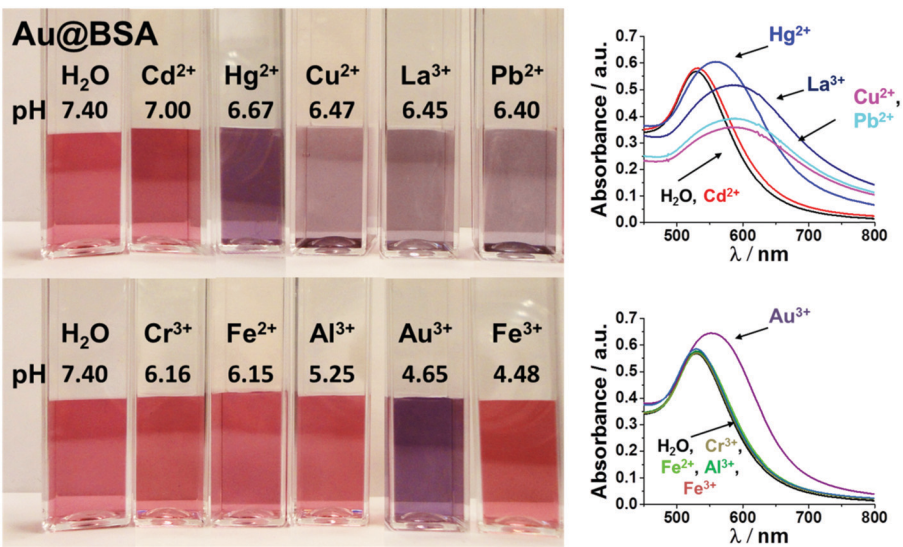

Fig. 2 Optical response of Au@BSA NPs towards di- and trivalent metal cations. Photographs and respective UV-Vis spectra of dispersions Au@BSA in the presence of various cations with decreasing pH from 6.7 to 4.5. The NP concentration for all dispersions is 0.15 mM Au(0) and the cation concentration is 100 μM. The photographs and the UV-Vis spectra were taken 30 min after the addition of the cations.

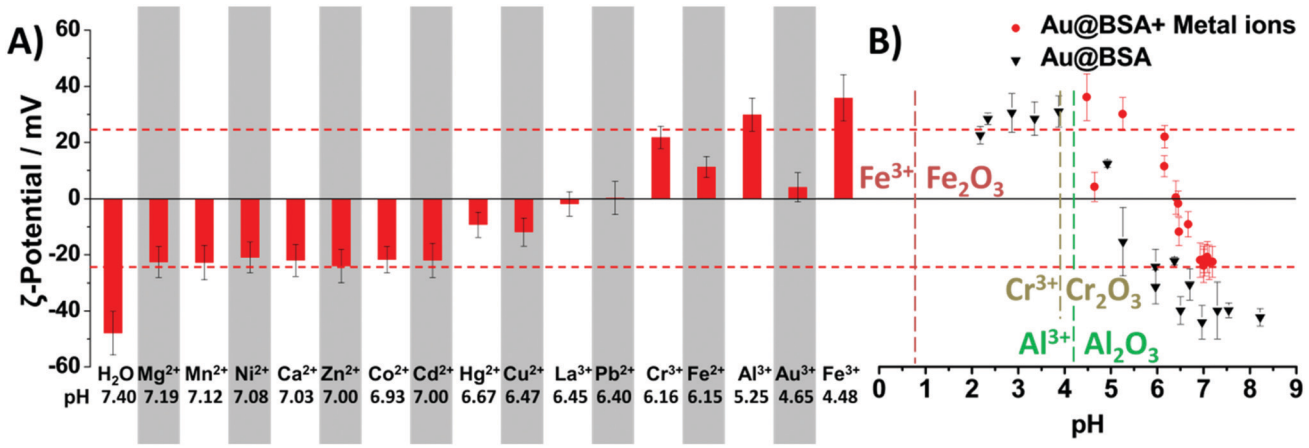

Fig. 3 (A) ζ-Potential and pH values of Au@BSA measured immediately after mixing them with various metal ions. The dashed lines (red) at the ζ-potential values of −25 and +25 mV indicate the stability threshold. (B) Comparison of the ζ-potential values of Au@BSA with Au@BSA after the incubation with several ions. The thermodynamic stable species of the ions and their conversion point (pH) into their (hydr)oxides was plotted for the type of ions for which charge inversion occurred, *e.g.*: Cr^{3+} (beige), Al^{3+}, (green) and $Fe^{2+/3+}$ (red).

Hg^{2+}, La^{3+} and Pb^{2+} we could detect a reduction of the ζ-potential up to around 0 mV which can explain the aggregation of the NPs.

A clear trend is visible when comparing the pH with the ζ-potential of Mg^{2+}, Mn^{2+}, Ni^{2+}, Ca^{2+}, Zn^{2+}, Co^{2+}, Cd^{2+}, Cu^{2+},

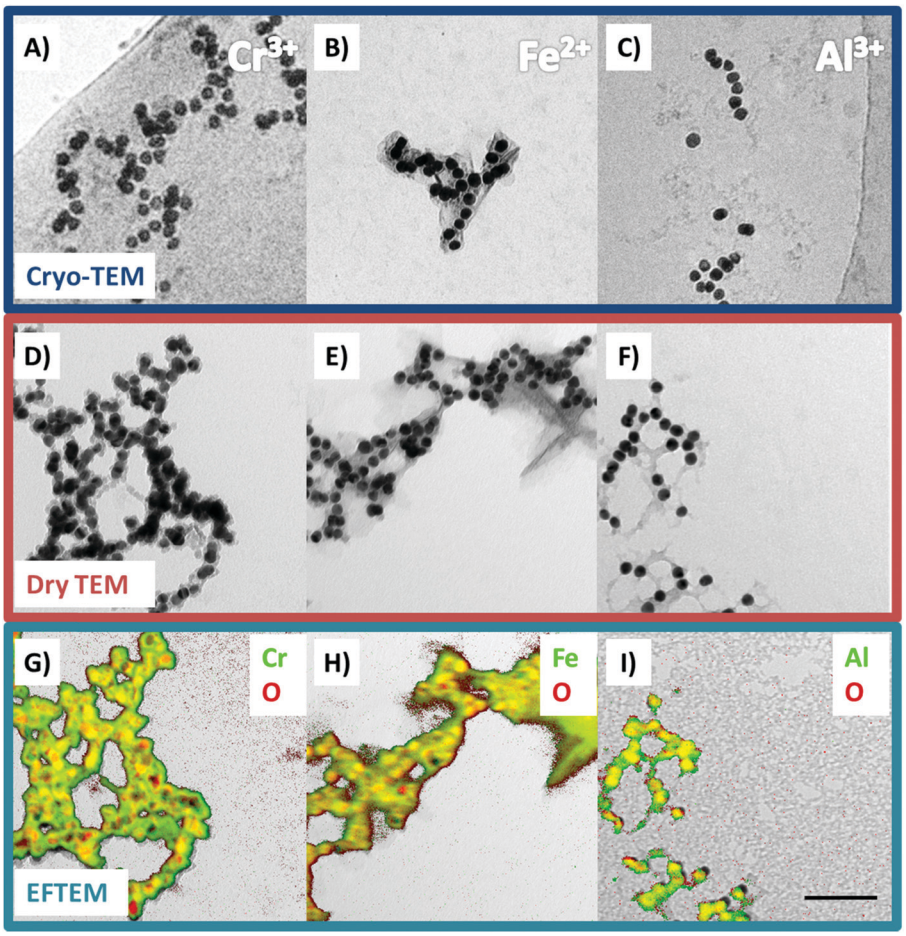

Fig. 4 Representative TEM micrographs of Au@BSA after the incubation with the metal ions that caused overcharging. (A–C) Cryo-TEM images of the Au@BSA NPs after the incubation with the metal ions. A grey shell can be seen around the Au@BSA NPs and in its surroundings. (D–F) Zero loss images of dried TEM samples which were used for the element mapping. (G–I) Element mapping (red = oxygen, green = metal ion, yellow = interference) by EFTEM which shows the presence of hydroxides in the grey shell. Scale bar is 100 nm.

Hg^{2+}, La^{3+} and Pb^{2+} (*cf.* Fig. 3). As expected, the ζ-potential decreases with decreasing pH. A comparison of these ζ-potentials with those of the pure Au@BSA NPs at the respective pH (*cf.* Fig. 3B), exhibits that the values after the interaction with ions are always lower than those of the pure Au@BSA NPs. That shows that the reduction in ζ-potential is not only due to the pH change, but also caused by charge screening of the ions.

Furthermore, positive ζ-potentials were measured for Fe^{2+}, Cr^{3+}, Al^{3+}, Au^{3+} and Fe^{3+}, *i.e.* a charge inversion occurred. Here the ζ-potential after the incubation with Au^{3+} is close to zero (4 ± 5 mV). For Fe^{2+} (11 ± 4 mV) and Cr^{3+} (22 ± 4 mV), the ζ-potential is below or close to the stability threshold of 25 mV, whereas for Al^{3+} (30 ± 6 mV) and Fe^{3+} (36 ± 8 mV), the ζ-potential values are above the stability threshold.

Overcharging of pure proteins is usually explained by the adsorption of ions at proteins.[1,5,33,50–62] However, this argumentation falls short, as the pre- and post-incubation pH has rarely been considered for Au@protein systems[63–65] or for pure proteins.[9,20] When the post incubation pH was measured, huge pH effects were observed that changed the protein charge drastically.[12–14,22]

As the pH is an important factor for the charge of proteins and thus also for Au@BSA NPs, the ζ-potential values must always be assessed in the context of the environmental pH. For Au^{3+} and Fe^{3+}, the pH lies below the isoelectrical point so that a charge inversion can be due to the pH change. Positive ζ-potential values at pH values above the isoelectrical point could be observed for Cr^{3+}, Fe^{2+} and Al^{3+} (*cf.* Fig. 3). As the isoelectrical point of our Au@BSA systems is around pH = 5,[40] these positive charges cannot solely be due to the changes of pH.

Therefore, this charge inversion must be due to the addition of cations or positively charged hydroxides.[28,66–69] Up to now, it is unknown whether adsorbed hydrolyzed ions[25–33] or adsorbed hydroxides[34–36] are responsible for overcharging. As the commonly used electrophoretic measurements *alone* cannot distinguish between hydrolyzed ions and hydroxides, the origin of charge inversion remains unclear.

The occurrence of hydroxides is ion specific and depends on the three parameters redox potential, ion concentration and pH. The boundaries of the thermodynamic stable species can be calculated for their respective parameters by using the Gibbs free energy and they can be visualized in Pourbaix diagrams.[7,70,71] The Pourbaix diagram shows the boundaries between metal ions and metal oxides, which occur as hydroxides in aqueous solution. Pourbaix diagrams are commonly used in engineering science to predict corrosion. To the best of our knowledge this is the first time that they are applied in the discussion of overcharging in colloidal science.

Fig. 3B shows the boundary pH values for Cr^{3+}, Fe^{2+} and Al^{3+} at the applied ion concentration of 100 μM and at the redox potentials of oxygen-saturated water. Oxygen saturation can be assumed as the experiments were conducted under ambient conditions. Fig. 3B shows that hydroxides can be expected for all of the three ions. As the hydroxides are positively charged at the given pH values[8] and the NPs are negatively charged, an interaction between the two occurring species can be expected.

To detect if adsorbed ions or adsorbed hydroxides are present and cause the overcharging, cryo-TEM and EFTEM was applied (*cf.* Fig. 4).

The cryo-TEM micrographs of Cr^{3+}, Fe^{2+} and Al^{3+} (Fig. 4A–C) show a grey shell around the Au@BSA NPs. This shell also connects the NPs with each other and is found in their further surroundings. In comparison to the cryo-TEM images of the pure Au@BSA NPs (*cf.* Fig. S1, ESI†), a significant increase of aggregates occurred. This can be due to the insufficient surface charge or it was caused by the charge inversion process. Charge inversion of colloids can generate aggregates, because NPs reach and cross the isoelectrical point, also known as the "point of zero charge". Here the charge repulsion is at a minimum and thus leads to aggregation.[72] To prove that the grey shell consists of hydroxides, we conducted element mapping of each respective ion and oxygen by energy filtered TEM. Au could not be mapped due to high energy loss edges (>2000 eV).[73] To visualize the results of the element mapping we overlayered the zero loss images (Fig. 4D–F) with the element maps (Fig. 4G–I). In the zero loss images the same grey shells could be observed as in the cryo-TEM measurements. The element mapping shows that the regions of

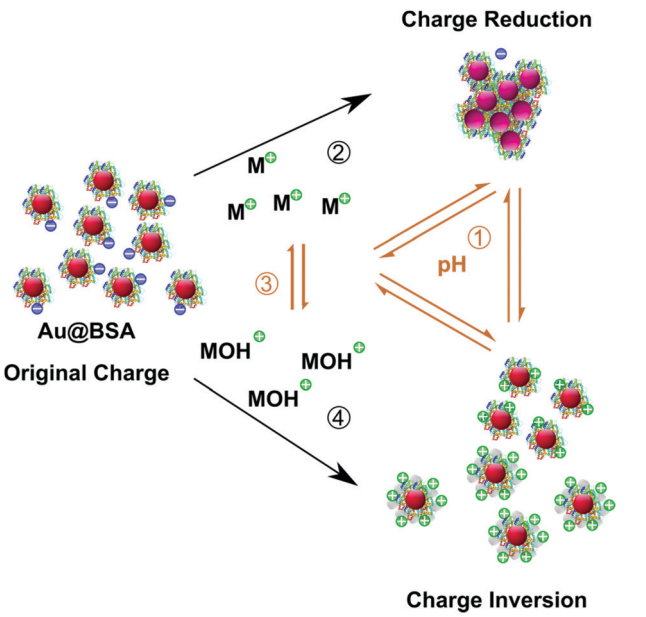

Scheme 1 Describing the effect of ions with Au@BSA NPS requires to take into account 4 different equilibriums, which are interconnected. Therein, the pH is the key parameter as it is involved in equilibrium 1 and 3 (brown color) directly. (1) The charge of Au@BSA NPs is influenced by the pH: above the isoelectrical point, the NPs are negatively charged and stable in dispersion, which is indicated by their red color. A reduction of the pH leads to aggregation around the isoelectrical point. The solution turns violet. Further reduction of the pH then leads to charge inversion, generating stable Au@BSA NPs again. (2) The charge of Au@BSA NPs can be screened by the addition of metal ions. Depending on the sort of ion and on the concentration, this can lead to aggregation. (3) The addition of metal ions can influence the pH. Depending on the pH, metal ions can convert into hydroxides. These hydroxides are positively charged at or below neutral pH. (4) For Cr^{3+}, Fe^{2+}, Al^{3+} overcharging is induced by a shell of absorbed hydroxides on the Au@BSA NPs.

the grey shell consist of oxygen and the respective metal ion. This proves that the outer shell of the colloids consists of hydroxides. As the outer shell determines the charge of a colloid these measurements prove that overcharging is due to hydroxides on the Au@BSA NPs.

Usually hydroxides are known to occur in the form of a white precipitate. As the hydroxide objects are below visible wavelength in this study, they could not be seen in the NPs' dispersion with the bare eye (*cf.* Fig. 2). These findings support the theory of hydroxides being responsible for the overcharging rather than hydrolyzed ions.[34–36]

3. Conclusion

We investigated the influence of metal ions being added to Au@BSA solution. Focus was put on the resulting pH and the charge of Au@BSA. The results are summarized in Scheme 1.

The surface charge of the Au@BSA NPs strongly depends on the pH (*cf.* Scheme 1.1 and Fig. 3B). The majority of the metal ions (*i.e.* Ca^{2+}, Mg^{2+}, Co^{2+}, Ni^{2+}, Mn^{2+}, Zn^{2+}, Cd^{2+}, Hg^{2+}, Cu^{2+}, La^{3+} and Pb^{2+}) show a pH reduction (*cf.* Scheme 1.3 and Fig. 3) and charge screening (*cf.* Scheme 1.2 and Fig. 3) which leads to a reduction in surface charge. A charge inversion from negative ζ-potential values to positive ζ-potential values was observed for Cr^{3+}, Fe^{2+}, Al^{3+}, Au^{3+} and Fe^{3+}. For these ions, the pH changed drastically from 7.4 to 6.16–4.48. For Cr^{3+}, Fe^{2+} and Al^{3+}, the pH values were well above of the isoelectrical point of Au@BSA, so that the pH cannot be the cause of the charge inversion. Pourbaix diagrams were used to show that at the respective pH of these ions, hydroxide formation can be expected (Fig. 3B and Scheme 1.3). For these systems, a shell of adsorbed hydroxides was found on the Au@BSA NPs (Scheme 1.4 and Fig. 4). As the hydroxides are positively charged below neutral pH, they render the Au@BSA NPs positive.

These results show that hydroxides – not unhydrolyzed or hydrolyzed ions – are responsible for the phenomenon of charge inversion. We showed that electrophoretical measurements alone (ζ-potential) cannot distinguish between the different species. To do so, it is necessary to combine those measurements with a microscopic technique such as TEM. Our findings provide fundamentally new insights into protein and metal ion interactions as well as into their correlations with the pH.

4. Experimental section

Chemicals

$HAuCl_4 \cdot 3H_2O$ ($\geq$99.9%), tri-sodium citrate dihydrate (>99%), bovine serum albumin (BSA), and all the metal salts ($\geq$99.0%) were purchased from Sigma-Aldrich. The solutions of metal ions were prepared from $CaCl_2 \cdot 2H_2O$, $MgCl_2 \cdot 6H_2O$, $ZnCl_2$, $CuCl_2 \cdot 2H_2O$, $Ni(NO_3)_2 \cdot 6H_2O$, $CoNO_3 \cdot 6H_2O$, $FeCl_2 \cdot 4H_2O$, $MnCl_2 \cdot 4H_2O$, $Pb(NO_3)_2$, $Cd(NO_3)_2 \cdot 4H_2O$, $HgCl_2$, $La(NO_3)_3 \cdot 6H_2O$, $AlCl_3 \cdot 6H_2O$, $CrCl_3$, $FeCl_3 \cdot 6H_2O$ by separately dissolving each compound in water. All chemicals were used as received. Milli-Q grade water was used in all preparations.

Synthesis of Au@protein NPs

Citrate coated Au NPs (Au@citrate) with an average particle size of 15 nm were synthesized by the Turkevich method.[74] The NPs were then coated with proteins by a simple ligand exchange process. For this, a protein–citrate solution was prepared with a concentration of 1 mg mL^{-1} protein and 0.1%$_{wt}$ citrate. The pH of the solution was then adjusted to 7–8 with NaOH. Subsequently, a 10-fold volume of citrate coated Au NPs ([Au] = 0.5 mM) were added under vigorous stirring. Resulting in a final protein concentration of 0.1 mg mL^{-1}. The mixture was stirred for 24 hours at room temperature. Finally, the protein coated Au NPs (Au@protein) were purified *via* 5-fold centrifugation (10 000*g*, 30 min) and stored at pH $\geq$ 9 at 4 °C.

Characterization

TEM images were acquired on a Libra 120 cryo-TEM from Carl Zeiss NTS GmbH equipped with a LaB6 source and an omega-type energy filter. The acceleration voltage was 120 kV. For TEM measurements, the samples were prepared by drop-coating 5 μL of the NPs' solution onto a carbon coated copper grid (CF200-Cu, Electron Microscopy Sciences, Hatfield, USA). After 10 min, residual solution was removed by blotting with a filter paper. Presence of iron, chrome, aluminum and oxygen and their spatial distribution were determined by electron energy loss spectroscopy (EELS) and energy filtered TEM imaging (EFTEM). UV-Vis-near-IR spectra were measured with a Cary 5000 UV-Vis-NIR spectrophotometer. ζ-Potential values were determined through electrophoretic mobility measurements using a Malvern Zetasizer Nano ZS by taking the average of five measurements, each consisting of 70 runs. pH measurements were performed with SI Analytics Lab 850 equipped with a N6280. The photographs were recorded with a Sony DSC-W350 digital camera.

Metal ion study of Au@protein NPs

Prior to the mixing of the metal ions with the Au@protein NPs (Au concentration = 0.15 mM), the pH of the NP dispersions were adjusted to pH 7.4 $\pm$ 0.1. Then 2 mL of the NP dispersion were given in a cuvette (polystyrene, 10 mm) and 20 μL of the dispersion was replaced by 20 μL of a freshly prepared 10 mM solution of each metal ion, resulting into the final metal ion concentration of 100 μM. The solutions were mixed directly in the cuvettes by pipetting the mixture up and down multiple times. Then UV-Vis spectra, photographs and the ζ-potential measurements were conducted.

Conflicts of interest

There are no conflicts to declare.

Acknowledgements

J. S. was supported and funded by a grant for PhD candidates of the German Federal Environmental Foundation (DBU). Petr Formanek for help with EM measurements, Anja Caspari for

zeta-potential measurements, Astrid Drechsler and Frank Simon for helpful discussions and Corinna Link, Julian Thiele, Alla Synytska, Max Schnepf, Roland Höller and Daniel Forberg for proof-reading. C. R. acknowledges support by the Elite Network of Bavaria (Study Program Biological Physics).

References

1 J. Lyklema, Quest for ion-ion correlations in electric double layers and overcharging phenomena, *Adv. Colloid Interface Sci.*, 2009, **147–148**, 205–213.
2 J. Lyklema, Overcharging, charge reversal: Chemistry or physics?, *Colloids Surf., A*, 2006, **291**(1–3), 3–12.
3 R. Kjellander, Ion-ion correlations and effective charges in electrolyte and macroion systems, *Ber. Bunsenges. Phys. Chem.*, 1996, **100**(6), 894–904.
4 J. Lyklema and T. P. Golub, *Electrical double layer on silver iodide and overcharging in the presence of hydrolyzable cations*, 2007, vol. 80, pp. 303–311.
5 H. I. Okur, J. Hladilkova, K. B. Rembert, Y. Cho, J. Heyda, J. Dzubiella, P. S. Cremer and P. Jungwirth, Beyond the Hofmeister Series: Ion-Specific Effects on Proteins and Their Biological Functions, *J. Phys. Chem. B*, 2017, **121**(9), 1997–2014.
6 H. Lyklema, 3 – Pair Interactions, in *Fundamentals of Interface and Colloid Science*, ed. J. Lyklema, Academic Press, 2005, vol. 4, p. 3.
7 N. Takeno, Atlas of Eh-pH diagrams, *Geological survey of Japan open file report 419*, 2005, p. 102.
8 M. Kosmulski, Isoelectric points and points of zero charge of metal (hydr)oxides: 50 years after Parks' review, *Adv. Colloid Interface Sci.*, 2016, **238**, 1–61.
9 M. K. Braun, M. Wolf, O. Matsarskaia, S. Da Vela, F. Roosen-Runge, M. Sztucki, R. Roth, F. Zhang and F. Schreiber, Strong Isotope Effects on Effective Interactions and Phase Behavior in Protein Solutions in the Presence of Multivalent Ions, *J. Phys. Chem. B*, 2017, **121**(7), 1731–1739.
10 M. Grimaldo, F. Roosen-Runge, M. Hennig, F. Zanini, F. Zhang, M. Zamponi, N. Jalarvo, F. Schreiber and T. Seydel, Salt-Induced Universal Slowing Down of the Short-Time Self-Diffusion of a Globular Protein in Aqueous Solution, *J. Phys. Chem. Lett.*, 2015, **6**(13), 2577–2582.
11 L. Ianeselli, F. Zhang, M. W. A. Skoda, R. M. J. Jacobs, R. A. Martin, S. Callow, S. Prévost and F. Schreiber, Protein–Protein Interactions in Ovalbumin Solutions Studied by Small-Angle Scattering: Effect of Ionic Strength and the Chemical Nature of Cations, *J. Phys. Chem. B*, 2010, **114**(11), 3776–3783.
12 E. Jordan, F. Roosen-Runge, S. Leibfarth, F. Zhang, M. Sztucki, A. Hildebrandt, O. Kohlbacher and F. Schreiber, Competing salt effects on phase behavior of protein solutions: tailoring of protein interaction by the binding of multivalent ions and charge screening, *J. Phys. Chem. B*, 2014, **118**(38), 11365–11674.
13 F. Roosen-Runge, B. S. Heck, F. Zhang, O. Kohlbacher and F. Schreiber, Interplay of pH and binding of multivalent metal ions: charge inversion and reentrant condensation in protein solutions, *J. Phys. Chem. B*, 2013, **117**(18), 5777–5787.
14 A. Sauter, F. Roosen-Runge, F. Zhang, G. Lotze, A. Feoktystov, R. M. Jacobs and F. Schreiber, On the question of two-step nucleation in protein crystallization, *Faraday Discuss.*, 2015, **179**, 41–58.
15 A. Sauter, F. Zhang, N. K. Szekely, V. Pipich, M. Sztucki and F. Schreiber, Structural Evolution of Metastable Protein Aggregates in the Presence of Trivalent Salt Studied by (V)SANS and SAXS, *J. Phys. Chem. B*, 2016, **120**(24), 5564–5571.
16 M. Wolf, F. Roosen-Runge, F. Zhang, R. Roth, M. W. A. Skoda, R. M. J. Jacobs, M. Sztucki and F. Schreiber, Effective interactions in protein–salt solutions approaching liquid–liquid phase separation, *J. Mol. Liq.*, 2014, **200**, 20–27.
17 F. Zhang, F. Roosen-Runge, A. Sauter, R. Roth, M. W. A. Skoda, R. M. J. Jacobs, M. Sztucki and F. Schreiber, The role of cluster formation and metastable liquid–liquid phase separation in protein crystallization, *Faraday Discuss.*, 2012, **159**, 313–325.
18 F. Zhang, F. Roosen-Runge, A. Sauter, M. Wolf, R. M. J. Jacobs and F. Schreiber, Reentrant condensation, liquid–liquid phase separation and crystallization in protein solutions induced by multivalent metal ions, *Pure Appl. Chem.*, 2014, **86**(2), 191–202.
19 F. Zhang, R. Roth, M. Wolf, F. Roosen-Runge, M. W. A. Skoda, R. M. J. Jacobs, M. Stzucki and F. Schreiber, Charge-controlled metastable liquid–liquid phase separation in protein solutions as a universal pathway towards crystallization, *Soft Matter*, 2012, **8**(5), 1313–1316.
20 F. Zhang, M. W. Skoda, R. M. Jacobs, S. Zorn, R. A. Martin, C. M. Martin, G. F. Clark, S. Weggler, A. Hildebrandt, O. Kohlbacher and F. Schreiber, Reentrant condensation of proteins in solution induced by multivalent counterions, *Phys. Rev. Lett.*, 2008, **101**(14), 148101.
21 F. Zhang, M. W. A. Skoda, R. M. J. Jacobs, R. A. Martin, C. M. Martin and F. Schreiber, Protein Interactions Studied by SAXS: Effect of Ionic Strength and Protein Concentration for BSA in Aqueous Solutions, *J. Phys. Chem. B*, 2007, **111**(1), 251–259.
22 F. Zhang, S. Weggler, M. J. Ziller, L. Ianeselli, B. S. Heck, A. Hildebrandt, O. Kohlbacher, M. W. Skoda, R. M. Jacobs and F. Schreiber, Universality of protein reentrant condensation in solution induced by multivalent metal ions, *Proteins*, 2010, **78**(16), 3450–3457.
23 C. A. Burns, J. F. Boily, R. J. Crawford and I. H. Harding, Cd(II) binding by particulate low-rank coals in aqueous media: sorption characteristics and NICA-Donnan models, *J. Colloid Interface Sci.*, 2004, **278**(2), 291–298.
24 M. Chanana, M. A. Correa-Duarte and L. M. Liz-Marzan, Insulin-coated gold nanoparticles: a plasmonic device for studying metal-protein interactions, *Small*, 2011, **7**(18), 2650–2660.
25 Y. E. Collins and G. Stotzky, Heavy metals alter the electrokinetic properties of bacteria, yeasts, and clay minerals, *Appl. Environ. Microbiol.*, 1992, **58**(5), 1592–1600.
26 R. J. Crawford, I. H. Harding and D. E. Mainwaring, The Zeta Potential of Iron and Chromium Hydrous Oxides

during Adsorption and Coprecipitation of Aqueous Heavy Metals, *J. Colloid Interface Sci.*, 1996, **181**(2), 561–570.

27 M. L. Jimenez, A. V. Delgado and J. Lyklema, Hydrolysis versus ion correlation models in electrokinetic charge inversion: establishing application ranges, *Langmuir*, 2012, **28**(17), 6786–6793.

28 W. H. Kuan, S. L. Lo and M. K. Wang, Modeling and electrokinetic evidences on the processes of the Al(III) sorption continuum in SiO_2(s) suspension, *J. Colloid Interface Sci.*, 2004, **272**(2), 489–497.

29 Y. Leong, Surface forces arising from adsorbed hydrolysis products of metal ions in ZrO_2 and silica dispersions: Cu(II), Ni(II), Co(II) and Al(III), *Powder Technol.*, 2007, **179**(1-2), 38–42.

30 L. Qian and B. Chen, Dual role of biochars as adsorbents for aluminum: the effects of oxygen-containing organic components and the scattering of silicate particles, *Environ. Sci. Technol.*, 2013, **47**(15), 8759–8768.

31 F. Rao, S. Song and A. Lopez-Valdivieso, Specific Adsorption of Chromium Species on Kaolinite Surface, *Miner. Process. Extr. Metall. Rev.*, 2012, **33**(3), 180–189.

32 K. Subramaniam, S. Yiacoumi and C. Tsouris, Copper uptake by inorganic particles—equilibrium, kinetics, and particle interactions: experimental, *Colloids Surf., A*, 2001, **177**(2), 133–146.

33 E. Wernersson, R. Kjellander and J. Lyklema, Charge Inversion and Ion–Ion Correlation Effects at the Mercury/Aqueous $MgSO_4$ Interface: Toward the Solution of a Long-Standing Issue, *J. Phys. Chem. C*, 2010, **114**(4), 1849–1866.

34 R. J. Hunter and M. James, Charge Reversal of Kaolinite by Hydrolyzable Metal-Ions - An Electroacoustic Study, *Clays Clay Miner.*, 1992, **40**(6), 644–649.

35 R. O. James and T. W. Healy, Adsorption of hydrolyzable metal ions at the oxide—water interface. II. Charge reversal of SiO_2 and TiO_2 colloids by adsorbed Co(II), La(III), and Th(IV) as model systems, *J. Colloid Interface Sci.*, 1972, **40**(1), 53–64.

36 W. Kuan, S. Lo and M. Wang, pH effect on the surface and bulk characteristics of metallic cations/SiO_2 suspensions, *Water Sci. Technol.*, 2000, **42**(3–4), 441–446.

37 I. Dewald, O. Isakin, J. Schubert, T. Kraus and M. Chanana, Protein Identity and Environmental Parameters Determine the Final Physicochemical Properties of Protein-Coated Metal Nanoparticles, *J. Phys. Chem. C*, 2015, **119**(45), 25482–25492.

38 R. P. Höller, M. Dulle, S. Thoma, M. Mayer, A. M. Steiner, S. Forster, A. Fery, C. Kuttner and M. Chanana, Protein-Assisted Assembly of Modular 3D Plasmonic Raspberry-like Core/Satellite Nanoclusters: Correlation of Structure and Optical Properties, *ACS Nano*, 2016, **10**(6), 5740–5750.

39 M. J. Männel, L. P. Kreuzer, C. Goldhahn, J. Schubert, M. J. Hartl and M. Chanana, Catalytically Active Protein Coatings: Towards Enzymatic Cascade Reactions at Inter-Colloidal Level, *ACS Catal.*, 2017, 1664–1672.

40 M. S. Strozyk, M. Chanana, I. Pastoriza-Santos, J. Pérez-Juste and L. M. Liz-Marzán, Protein/Polymer-Based Dual-Responsive Gold Nanoparticles with pH-Dependent Thermal Sensitivity, *Adv. Funct. Mater.*, 2012, **22**(7), 1436–1444.

41 M. Tebbe, C. Kuttner, M. Mannel, A. Fery and M. Chanana, Colloidally stable and surfactant-free protein-coated gold nanorods in biological media, *ACS Appl. Mater. Interfaces*, 2015, **7**(10), 5984–5991.

42 M. Chanana, P. Rivera_Gil, M. A. Correa-Duarte, L. M. Liz-Marzán and W. J. Parak, Physicochemical Properties of Protein-Coated Gold Nanoparticles in Biological Fluids and Cells before and after Proteolytic Digestion, *Angew. Chem., Int. Ed.*, 2013, **52**(15), 4179–4183.

43 L. P. Kreuzer, M. J. Männel, J. Schubert, R. P. M. Höller and M. Chanana, Enzymatic Catalysis at Nanoscale: Enzyme-Coated Nanoparticles as Colloidal Biocatalysts for Polymerization Reactions, *ACS Omega*, 2017, **2**(10), 7305–7312.

44 D. Malamud and J. W. Drysdale, Isoelectric points of proteins: a table, *Anal. Biochem.*, 1978, **86**(2), 620–647.

45 P. G. Righetti and T. Caravaggio, Isoelectric points and molecular weights of proteins: A table, *J. Chromatogr. A*, 1976, **127**(1), 1–28.

46 P. Debye and E. Hückel, Zur Theorie der Elektrolyte, *Phys. Z.*, 1923, **24**(9), 185–206.

47 J. Lyklema, *Solid-Liquid Interfaces, Fundamentals of Interface and Colloid Science*, Academic Press, San Diego, CA, 1995, vol. I.

48 R. Pashley and M. Karaman, *Applied colloid and surface chemistry*, John Wiley & Sons, 2005.

49 J. Lyklema, *Fundamentals of interface and colloid science: soft colloids*, Elsevier, 2005, vol. 5.

50 A. Y. Grosberg, T. Nguyen and B. Shklovskii, Colloquium: the physics of charge inversion in chemical and biological systems, *Rev. Mod. Phys.*, 2002, **74**(2), 329–343.

51 J. Faraudo and A. Travesset, The Many Origins of Charge Inversion in Electrolyte Solutions: Effects of Discrete Interfacial Charges, *J. Phys. Chem. C*, 2007, **111**(2), 987–994.

52 Z. Y. Wang, Charge reversal at a planar boundary between two dielectrics, *Phys. Rev. E*, 2016, **93**(1), 012605.

53 M. Trulsson, B. Jonsson, T. Akesson, J. Forsman and C. Labbez, Repulsion between oppositely charged surfaces in multivalent electrolytes, *Phys. Rev. Lett.*, 2006, **97**(6), 068302.

54 I. Semenov, S. Raafatnia, M. Sega, V. Lobaskin, C. Holm and F. Kremer, Electrophoretic mobility and charge inversion of a colloidal particle studied by single-colloid electrophoresis and molecular dynamics simulations, *Phys. Rev. E: Stat., Nonlinear, Soft Matter Phys.*, 2013, **87**(2), 022302.

55 A. P. Dos Santos, A. Bakhshandeh, A. Diehl and Y. Levin, Adsorption isotherms of charged nanoparticles, *Soft Matter*, 2016, **12**(41), 8528–8533.

56 S. Raafatnia, O. A. Hickey, M. Sega and C. Holm, Computing the electrophoretic mobility of large spherical colloids by combining explicit ion simulations with the standard electrokinetic model, *Langmuir*, 2014, **30**(7), 1758–1767.

57 S. Raafatnia, O. A. Hickey and C. Holm, Mobility reversal of polyelectrolyte-grafted colloids in monovalent salt solutions, *Phys. Rev. Lett.*, 2014, **113**(23), 238301.

58 C. Pasquier, M. Vazdar, J. Forsman, P. Jungwirth and M. Lund, Anomalous Protein-Protein Interactions in Multivalent Salt Solution, *J. Phys. Chem. B*, 2017, **121**(14), 3000–3006.

59 R. Messina, Electrostatics in Soft Matter, *J. Phys.: Condens. Matter*, 2008, **21**(19), 199801.
60 M. Kohagen, E. Pluharova, P. E. Mason and P. Jungwirth, Exploring Ion-Ion Interactions in Aqueous Solutions by a Combination of Molecular Dynamics and Neutron Scattering, *J. Phys. Chem. Lett.*, 2015, **6**(9), 1563–1567.
61 E. A. Barrios-Contreras, E. González-Tovar and G. I. Guerrero-García, The dominance of small ions in the electric double layer of size- and charge-asymmetric electrolytes: a mean-field study on the charge reversal and surface charge amplification, *Mol. Phys.*, 2015, **113**(9–10), 1190–1205.
62 A. I. Abrikosov, B. Stenqvist and M. Lund, Steering patchy particles using multivalent electrolytes, *Soft Matter*, 2017, **13**(26), 4591–4597.
63 R. M. Tripathi, R. K. Gupta, P. Singh, A. S. Bhadwal, A. Shrivastav, N. Kumar and B. R. Shrivastav, Ultra-sensitive detection of mercury(II) ions in water sample using gold nanoparticles synthesized by Trichoderma harzianum and their mechanistic approach, *Sens. Actuators, B*, 2014, **204**, 637–646.
64 D.-Y. Kim, S. Shinde, R. Saratale, A. Syed, F. Ameen and G. Ghodake, Spectrophotometric determination of Fe(III) by using casein-functionalized gold nanoparticles, *Microchim. Acta*, 2017, **184**(12), 4695–4704.
65 Y. Guo, Z. Wang, W. Qu, H. Shao and X. Jiang, Colorimetric detection of mercury, lead and copper ions simultaneously using protein-functionalized gold nanoparticles, *Biosens. Bioelectron.*, 2011, **26**(10), 4064–4069.
66 S. Acar and P. Somasundaran, Effect of dissolved mineral species on the electrokinetic behaviour of sulfides, *Miner. Eng.*, 1992, **5**(1), 27–40.
67 K. K. Das, Pradip and K. A. Natarajan, The Effect of Constituent Metal Ions on the Electrokinetics of Chalcopyrite, *J. Colloid Interface Sci.*, 1997, **196**(1), 1–11.
68 S. B. Johnson, D. R. Dixon and P. J. Scales, The electrokinetic and shear yield stress properties of kaolinite in the presence of aluminium ions, *Colloids Surf., A*, 1999, **146**(1), 281–291.
69 L. K. Witika and B. Dobias, Electrokinetics of sulphide minerals: Fundamental surface reactions of carrollite, *Miner. Eng.*, 1993, **6**(8), 883–894.
70 K. A. Persson, B. Waldwick, P. Lazic and G. Ceder, Prediction of solid-aqueous equilibria: Scheme to combine first-principles calculations of solids with experimental aqueous states, *Phys. Rev. B: Condens. Matter Mater. Phys.*, 2012, **85**, 23.
71 M. Pourbaix, *Atlas of electrochemical equilibria in aqueous solution*, NACE, 1974, vol. 307.
72 G. B. Sukhorukov, E. Donath, S. Davis, H. Lichtenfeld, F. Caruso, V. I. Popov and H. Möhwald, Stepwise polyelectrolyte assembly on particle surfaces: a novel approach to colloid design, *Polym. Adv. Technol.*, 1998, **9**(10–11), 759–767.
73 C. C. Ahn, *Transmission electron energy loss spectrometry in materials science and the EELS atlas*, John Wiley & Sons, 2006.
74 J. Turkevich, P. C. Stevenson and J. Hillier, A study of the nucleation and growth processes in the synthesis of colloidal gold, *Discuss. Faraday Soc.*, 1951, **11**, 55–75.